Title
A Mechanism of Land Degradation in Turf-Mantled Slopes of the Tibetan Plateau

Journal
Geophysical Research Letters, 45(9)

ISSN
0094-8276

Authors
Okin, Gregory S
D'Odorico, Paolo
Liu, Jianquan

Publication Date
2018-05-16

DOI
10.1029/2018gl077055

Peer reviewed

Geophysical Research Letters

RESEARCH LETTER
10.1029/2018GL077055

Key Points:
- *Kobresia pygmaea* turf systems are bistable, with vegetated/protected and unvegetated/erosive stable states
- Degradation of *Kobresia pygmaea* turfs occurs due to channelization of flow into preexisting cracks, which are widened by erosion
- Degradation of the world's most extensive alpine ecosystem has implications for erosion and sediment delivery in headwaters of Asia's major rivers

Supporting Information:
- Supporting Information S1

Correspondence to:
G. S. Okin,
okin@geog.ucla.edu

Citation:
Okin, G. S., D'Odorico, P., & Liu, J. (2018). A mechanism of land degradation in turf-mantled slopes of the Tibetan Plateau. *Geophysical Research Letters*, *45*, 4041–4048. https://doi.org/10.1029/2018GL077055

Received 16 JAN 2018
Accepted 10 APR 2018
Accepted article online 19 APR 2018
Published online 4 MAY 2018

A Mechanism of Land Degradation in Turf-Mantled Slopes of the Tibetan Plateau

Gregory S. Okin[1], Paolo D'Odorico[2], and Jianquan Liu[3]

[1]Department of Geography, University of California, Los Angeles, CA, USA, [2]Department of Environmental, Science, Policy and Management, University of California, Berkeley, CA, USA, [3]State Key Laboratory of Grassland Agro-Ecosystem, School of Life Science, Lanzhou University, Lanzhou, China

Abstract *Kobresia pygmaea* meadows are typical of Tibetan Plateau landscapes in the 3,000 to 5,500 m elevation range and constitute the most extensive alpine ecosystem in the world. *Kobresia pygmaea* forms turf mats that stabilize the surface and shelter the underlying soils from water erosion. Large tracts of the Plateau, however, exhibit signs of ongoing degradation of the turf and erosion of the underlying soil. Despite the crucial role played by *K. pygmaea* turf mats in the stabilization of the headwaters of major Asian rivers, the mechanisms responsible for their degradation remain poorly investigated. Here we develop a process-based model of land degradation of Tibetan Plateau slopes, which accounts for (i) turf cracking, (ii) water flow concentration in the cracks, (iii) crack widening by scouring, and (iv) sheet-flow erosion. As expected, soil erosion increases with the slope and drainage area (hence the observation of stronger erosion in relatively steep downhill sites). Model simulations indicate that with a sensible set of parameters representative of soil and hydrologic conditions in the region, Tibetan Plateau landscapes are vulnerable to turf mat degradation and soil erosion. As soon as polygonal cracks develop, water flow widens them until the landscape is completely barren. At this point sheet flow eventually erodes the mineral soil leaving behind a highly degraded landscape.

Plain Language Summary *Kobresia pygmaea* constitute the most extensive alpine ecosystem in the world and, in addition to providing forage for grazing animals also protect hillslopes from erosion. In this study, we hypothesize a mechanism for the breakup of these mats and present a mathematical model for this process. Our model shows that the stability of *K. pygmaea* turf mats depends upon slope and precipitation with time for denudation of the turfs at the base of slopes ranging from decades to centuries. We suggest that these mats may be bistable, with clear mechanisms for degradation but no clear mechanisms for regeneration of the mats.

1. Introduction

Kobresia pygmaea meadows are the largest alpine ecosystem in the world and are almost ubiquitous in the Tibetan Plateau with a total area of 450,000 km^2. They are mainly found in the southeastern Tibetan highlands in high alpine pastures in the region. Their elevation range is between 3,000 and 5,500 m above sea level, in areas with mean annual rainfall in the 200–1,000 mm/year range (Figure 1; Miehe et al., 2008).

Kobresia pygmaea meadows are undergoing changes as a result of climate warming and (possibly) overgrazing, which act at different stages of the degradation process. To date, more than three fourths of *K. pygmaea* meadows exhibit discontinuous cover, with patchy landscapes dissected by soil cracks and eroding trenches of different widths, depending on the degradation stage. Although possibly unstable, these areas of fragmented turf tend to exhibit *K. pygmaea* communities with higher diversity (e.g., Miehe et al., 2008). The role of livestock (yaks) in the erosion of *K. pygmaea* patches (e.g., Holzner & Kriechbaum, 1998) has been recently challenged. In fact, it has been argued that degradation is not related to trampling by yaks because there is evidence that *K. pygmaea* degradation is ongoing although grazing density is presently down (Miehe et al., 2008). Further, warming, not grazing, decreases rangeland quality in these meadows (Klein et al., 2007).

Kobresia pygmaea forms firm and continuous turf mats, about 10 cm thick, that stabilize the surface and shelter the underlying soils from erosion. *Kobresia pygmaea* grows less than 2 cm tall and is palatable to livestock. The turf remains frozen in the winter months and thaws in the late spring and summer seasons, with frequent nocturnal freezing in the spring and part of the summer, depending on the elevation (Xiong et al., 2014). The

Figure 1. Spatial distribution (shaded) of *K. pygmaea* meadows (after Miehe et al., 2014).

turf mat insulates the underlying soil thereby reducing the frequency of nocturnal soil freezing during the growing season. As noted above, turf mats protect and stabilize the underlying (typically thin) mineral soil layer. The fact that the turf has established at least over the last several thousand years, likely in response to early grazing by domesticated animals on the Plateau (from Miehe et al., 2014), suggests that the turf is stable with respect to erosion if it is not cracked.

Kobresia pygmaea turf degrades in a sequence of processes illustrated in Figure 2. The turf mat is first dissected into pseudo-hexagons (typically ≈0.5–2 m diameter) by tension cracking (Lachenbruch, 1961). Turf cracking results from desiccation processes associated with climate change (Miehe et al., 2008). Crack incision by runoff water and other processes leads to the progressive scouring of the edges of these polygons and the consequent increase in the spatial extent of eroded (bare mineral soil) areas. As they widen, cracks connect, thus increasing the connectivity of water and sediment transport pathways. This allows increased flow and begins the process of erosion of the underlying mineral soil, which accelerates breakup of the turf through undercutting. A hillslope becomes a mosaic of turf pedestals and clumps that eventually disappear through erosion, leaving behind bare mineral soil with little organic matter that is prone to sheet erosion. Turf cracking into hexagons can be observed at valley bottoms; likewise, soil denudation that is due to erosion of the hexagons can be observed only on sloping areas (Miehe et al., 2008).

The purpose of this study is to model the breakup and erosion of *K. pygmaea* turfs to help constrain the timescale for the degradation of these soils under different conditions and to estimate changes in erosion rate upon their degradation.

2. Methods

The model is developed to represent the states in turf degradation observed in the field (e.g., Figure 2). Code in the Interactive Data Language (IDL) is provided in supporting information (Text S1). The initial condition of

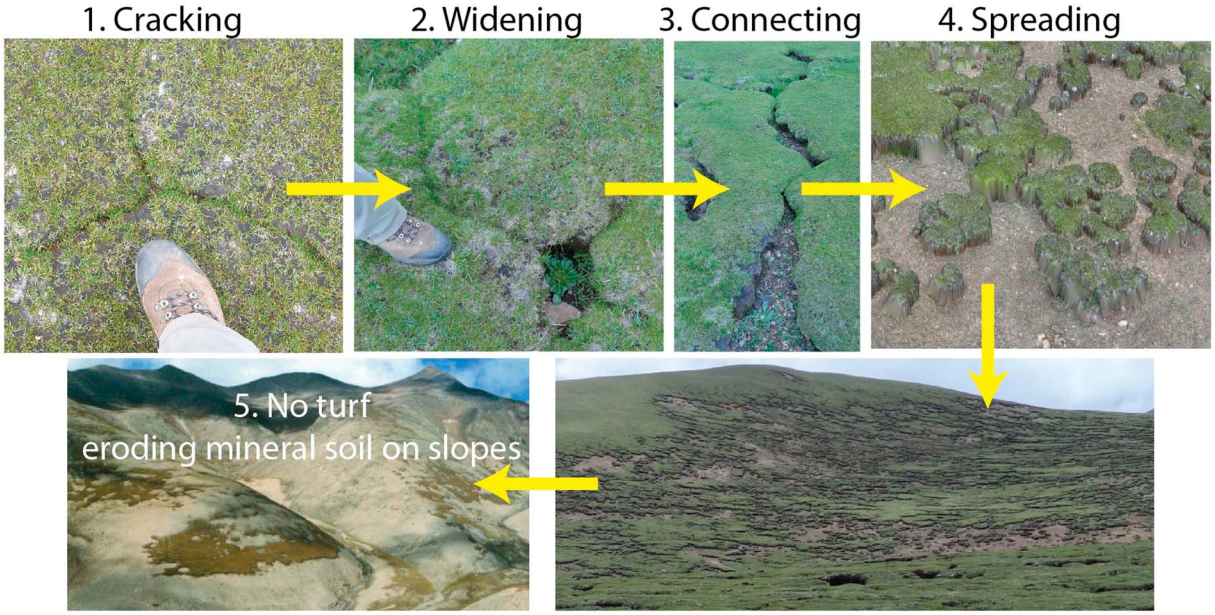

Figure 2. Observed phases in the breakup and degradation of *K. pygmaea* turf: Degradation starts with cracking (1) from desiccation, as cracks widen due to erosion of the edges of the turf (2), connectivity increases (3), allowing further erosion of the turf at the edges, (4) with eventual loss of turf and sheet or gully erosion of the underlying mineral soil (Miehe et al., 2008).

the model is a slope with turf that has experienced hexagonal cracking (Phase 1, Figure 2). Sheet flow over the turf concentrates into the cracks, initially assumed to be 1 cm wide, which are all connected. When and where the shear stress exerted by the water flow exceeds the shear strength of the underlying sediment, erosion occurs. This set of processes leads to reduction of the size, w, of the turf hexagons (Figure 3). The rate of erosion in the channel depends upon water flow through each channel, Q_w, which is calculated as

$$Q_w = A\,P/D, \tag{1}$$

where A is area contributing water to a point, P is the depth of a rain event, and D is the duration of a rain event. Rain depth and duration are each represented as exponentially distributed random variables, with mean $\overline{P}$ and $\overline{D}$, respectively (e.g., Rodriguez-Iturbe et al., 1987). Because the rain depth, P, is (nonlinearly) related to the rain duration, D—particularly in the case of extreme events, whose intensity typically decreases with the duration—P and D are simulated as correlated random variables (e.g., Kottegoda & Rosso, 1997; Koutsoyiannis & Foufoula-Georgiou, 1993): For each rain event D is randomly sampled with exponential distribution with mean $\overline{D}$; P is then sampled from an exponential distribution with mean $P^* = \overline{P}\left(\frac{D}{\overline{D}}\right)^m$, where P^* is the conditional mean of P, given D, and m is the exponent of the depth-duration scaling law that in most climates is in the range 0.3–0.5 and is here taken equal to 0.4. $\overline{P}$ and $\overline{D}$ are set to 6 mm and 4 hr, respectively, based on data in Zhou et al. (2008).

The velocity of the flow in the channel, U, is given by

$$U = Q_w/b\,h, \tag{2}$$

where b is the width of the channel and h is the flow depth. Both b and h are dynamical variables; changes in b are associated with the erosion process (see equation (7), below), while changes in h are due to the different discharge values resulting from rainfall events of different magnitude. The values of h are calculated by solving for h the Manning's equation (see below).

Based on simple geometric considerations, it can be shown that the area drained at each connecting node, A, is equal to nA_1, where A_1 is the area of a single hexagonal patch (i.e., a hexagon of turf plus one-half of the surrounding channels or the area of hexagons before widening) and l is the length (here, 1 m) of the side of the hexagons before channel widening (Figure 3).

Hexagons above node 4C	Number of Hexagons	x	Each Hexagon Contributes	=	Contribution from Each Row
4	4	x	1/4	=	1
3	3	x	1/3	=	1
2	2	x	1/2	=	1
1	1	x	1	=	1
			Sum for 4th Order Node, 4C:		4

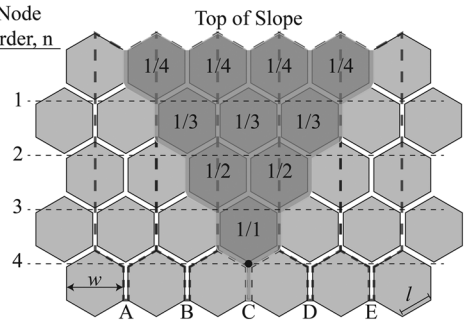

Figure 3. Geometric considerations for determining the contributing area, $A = nA_1$ where A_1 is the area of a single hexagonal patch. w is the hexagon width. l is initial hexagon side length. Two approaches yielding the same result are shown. In the first approach, nonoverlapping areas for fourth-order nodes 4A, 4B, 4C, 4D, and 4E are outlined in dashed lines. In each dashed area, there are four total hexagons. In the second approach, each hexagon that contributes water is labeled by the amount of water contributed. For the node, 4C (black circle), there is one hexagon just above that contributes all of its water; there are two hexagons above that that each contribute half of their water, and so on (see calculations on left).

The flow depth, h, is calculated in the channel as a function of Q_w and the slope, S, using Manning's uniform flow equation ($Q_w = n^{-1} b h R_H^{2/3} S^{1/2}$) with a value of Manning's roughness parameter, n, of 0.03 s m$^{-1/3}$ (e.g., Chow, 1959), where R_H is the hydraulic radius:

$$R_H = bh/(2\,h + b). \tag{3}$$

The shear stress exerted by the water flow, τ_s, is then calculated as

$$\tau_s = \rho_w\, g\, R_H\, S \tag{4}$$

where ρ_w is the density of water and g is the acceleration due to gravity.

Erosion occurs when τ_s exceeds a critical value, τ_c, which depends on soil cohesion (c_s), the additional cohesion effect (σ_s) of the grass turf (Hoffmans et al., 2009):

$$\tau_c = 0.056\,\left[g\,(\rho_s - \rho_w)\,d + c_s + \sigma_g\right], \tag{5}$$

where ρ_s is the density of the mineral soil or gravel particles (2.5 g/cm^3) and d is the average particle size of the erodible soil underlying the turf. Soil cohesion (c_s) varies as a function of texture, and in the case of unstructured clay soils can be in the 0–110 Pa range. The cohesion effect induced by the turf is typically stronger and depends on root strength and density and varies between σ_g = 2.8–11.2 kPa (Hoffmans et al., 2009). In this case σ_g is taken equal to zero because erosion occurs in the clayey organic layer below the grass roots.

The thickness, δ, of the sediment removed in channel widening on each side of the channel to the height of the water depth during an event of duration D can be determined following Hoffmans et al. (2009):

$$\delta = D\,E/(\rho_s\,(\tau_s - \tau_c)/\tau_c), \tag{6}$$

where E is the soil's intrinsic erodibility, typically in the range 1×10^{-5}–5×10^{-5} kg · m^{-2} · s^{-1}. After each eroding event, the channel is widened by 2δ (i.e., 1δ on both sides). Thus, the rates of channel widening and hexagon narrowing during an erosive event can be expressed as

$$\frac{db}{dt} = \frac{2\delta}{D} = \frac{2E\tau_c}{\rho_s(\tau_s - \tau_c)} \text{ and } \frac{dw}{dt} = -\frac{db}{dt} = -\frac{2E\tau_c}{\rho_s(\tau_s - \tau_c)}, \tag{7}$$

respectively. The undercutting that occurs on the turf is assumed to also result in the loss of overlying turf through some undefined process of mass wasting. In reality, frost heaving and trampling of the edge by yaks likely contribute to the collapse of the overlying turf. This material is assumed to not fill or block the channel, and due to its very high carbon content, it is assumed that it oxidizes rather than contributing to deposition.

As the hexagons get smaller, flow will transition from channelized to sheet flow. Therefore, we have modeled sheet erosion, A_{RUSLE}, using the Revised Universal Soil Loss Equation (RUSLE; Renard et al., 1991). Equations used for the RUSLE calculations are given in Table 1. Generally, though, the slope length and steepness factors in RUSLE, L_{RUSLE} and S_{RUSLE}, respectively, were calculated using the same slopes as above and the

Table 1
Equations Used for Event-Based Calculations of RUSLE Erosion, A_{RUSLE}

Parameter	RUSLE factor	Equations	Equation #
A_{RUSLE}	Erosion	$A_{RUSLE} = R_{RUSLE}K_{RUSLE}L_{RUSLE}S_{RUSLE}C_{RUSLE}P_{RUSLE}$	1–2
R_{RUSLE}	Erosivity	$R_{RUSLE} = E\,i$,	B-1
		for a single event, where E is rainstorm kinetic energy: $E = 1099D(1 - 0.72e^{-1.27i})$, and where i is maximum 30-m rainstorm intensity: $i = c\,P/D$	B-2 and B-3
K_{RUSLE}	Erodibility	$K_{RUSLE} = 7.594(0.0034 + 0.0405\,k)$ where $k = e^{-0.5([\mathrm{Log}(Dg)+1.659]/0.7101)^2}$	3–5
L_{RUSLE}	Length	$L_{RUSLE} = (l\cos(\theta)/c)^{\beta/(1+\beta)}$	4–1
		where c is 22 m, l is the distance, parallel to the slope, from the bottom of the slope to bottom-most hexagon with width $w \geq 25$ cm in meters, $\beta = (\sin\theta/0.0896)/(3(\sin\theta)^{0.8} + 0.56)$ and, $\theta = \tan^{-1}(S)$ where S is slope	4–3
S_{RUSLE}	Steepness	$S_{RUSLE} = 10.8\sin\theta + 0.03$	4–7
C_{RUSLE}	Cover	$C_{RUSLE} = 1$	n/a
P_{RUSLE}	Practices	$P_{RUSLE} = 1$	n/a

Note. Equation # refers to the equation number in Renard et al. (1997), where applicable.

distance from the bottom of the slope to the bottom-most hexagon with width $w \geq 25$ cm. The soil erodibility factor, K_{RUSLE}, was calculated using a geometric average particle diameter ($D_g = 0.26$ mm) that corresponds to the arithmetic average particle diameter (d = 0.86 mm) used above. For each rain event, the maximum 30-min intensity is calculated as the average intensity (P/D) times a multiplier, c, given by

$$c = 2D\frac{1 - e^{-0.5q/D}}{1 - e^{-q}}, \tag{8}$$

where q is a nonuniformity parameter (Brown & Foster, 1987). q was given a value of 10, a median of values given in Brown and Foster (1987) for 54 natural storms, resulting in a value of c of 6. This intensity is used for calculation of the RUSLE storm erosivity, EI, and rainfall-runoff intensity factor, R_{RUSLE}. The cover management, C_{RUSLE}, and support practice factors, P_{RUSLE}, were set to unity.

Each iteration of the model represents one rain event. The daily probability of rain is 7.4%, which is derived from the observations in Zhou et al. (2008) that the frequency of rain is ~0.30 per day during the summer months. Precipitation outside of the summer months is assumed to occur as solid precipitation, which infiltrates into the soil when it melts without causing erosion. The main output of the model with time is

Table 2
Parameters Used in this Study

Parameter	Value
Soil erodibility	$E = 1.5 \times 10^{-5}$ kg · m^{-2} · s^{-1}
Soil cohesion	$c_s = 40$ Pa
Cohesion effect of roots	$\sigma_g = 0$ Pa
Average soil grain size	$d = 0.86$ mm
Geometric average soil grain size	$D_g = 0.26$ mm
Soil grain density	$\rho_s = 2/5$ g cm^{-3}
Manning's roughness	$n = 0.03$ s m$^{-1/3}$
Average storm size	$\overline{P} = 6$ mm
Average storm duration	$\overline{D} = 4$ hr
Slope	$S = 0.15$ (unless otherwise indicated)
Rainfall nonuniformity parameter (equation (8)).	$q = 10$

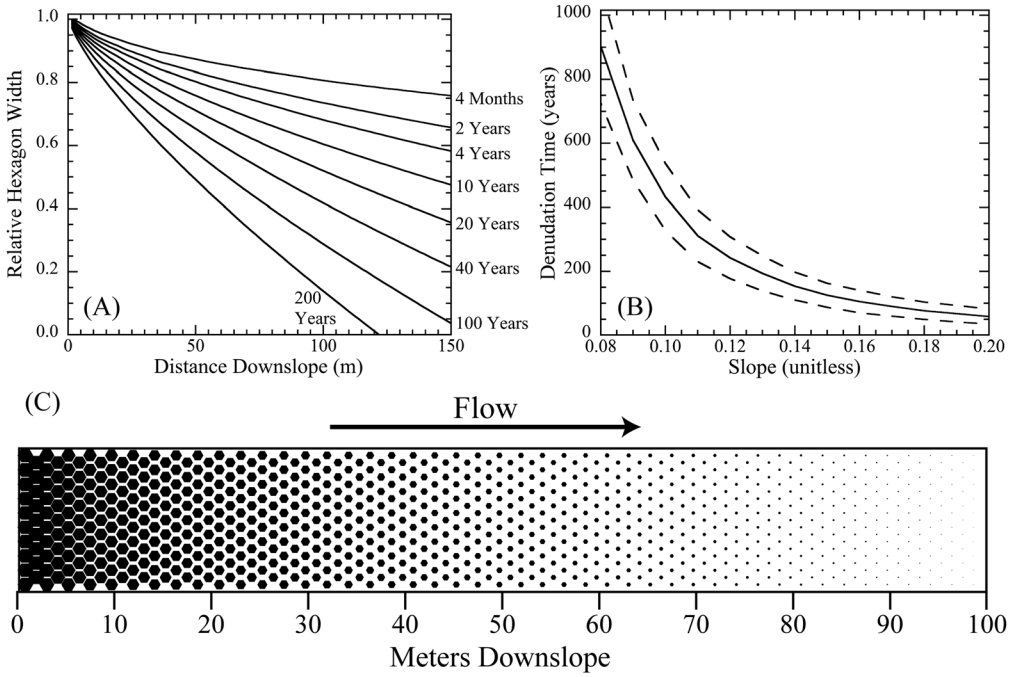

Figure 4. (a) Average hillslope profiles of hexagon width (relative to initial width) in a 200 3 year run (n = 100 [150-m slope]; slope = 0.15). (b) Denudation time as a function of slope (solid line) plus and minus one standard deviation (dashed lines), calculated for a slope that is 200 hexagons long (300-m slope) from 150 stochastic model simulations. (c) Visualization of hexagons for one realization of the model after 200 years with slope 0.15. The dark areas represent turf.

hexagon width, w, from which visualizations of the hexagons can be made. In addition, as an index of how fast the turf breakup process occurs, we calculate the "degradation time," T_d, the time that the lowest hexagon on the slope is smaller than 25 cm in maximum width. Due to the stochastic nature of the simulations, all results shown are the average values among 150 runs. The parameters used in the simulations are summarized in Table 2.

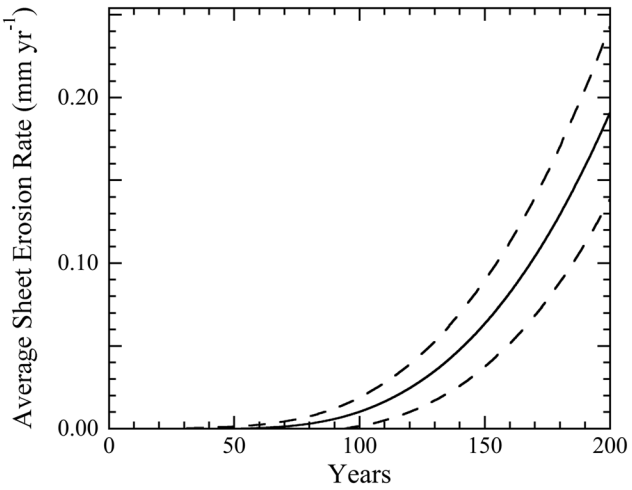

Figure 5. Average sheet erosion rate calculated for a 300-m slope (n = 200) over 200 years for a hillslope with slope 0.15. Sheet erosion is calculated when hexagons at the bottom of the slope are eroded to ≤25 cm, which occurred on average at 70 years. Other parameters same as in Table 2.

3. Results

Despite the simplistic representation of erosion in the model, it reproduces several features expected for the system. Degradation of the turf hexagons is most intense at the foot of the slope, and after several years, portions of the slope have no turf at all (Figure 4).

Our model indicates that initial erosion of the hexagons can occur quite rapidly, after a few particularly intense rain events. By the end of two to three years, the hexagons at the bottom of a 150-m slope can be <60% of their original size (Figure 4a). Within about 100–200 years, the sites at the bottom of a slope can be devoid of turf (Figures 4a and 4b).

The time required for hexagons to disappear from the bottom of a slope depends upon slope length, with longer slopes experiencing shorter degradation times because of the higher water flow (Figure 4a). The denudation time is a nonlinear function of slope (Figure 4c). Low slopes (<0.08) lead to complete turf degradation in more than 800 years for a slope with maximum order 200 (~300 m). Steeper slopes experience complete turf degradation at the bottom in several decades. After denudation of the turf at the bottom of the slope, sheet erosion begins and increases nonlinearly (Figure 5), taking 60–70 years for sheet erosion to initiate at the bottom of a 300-m slope.

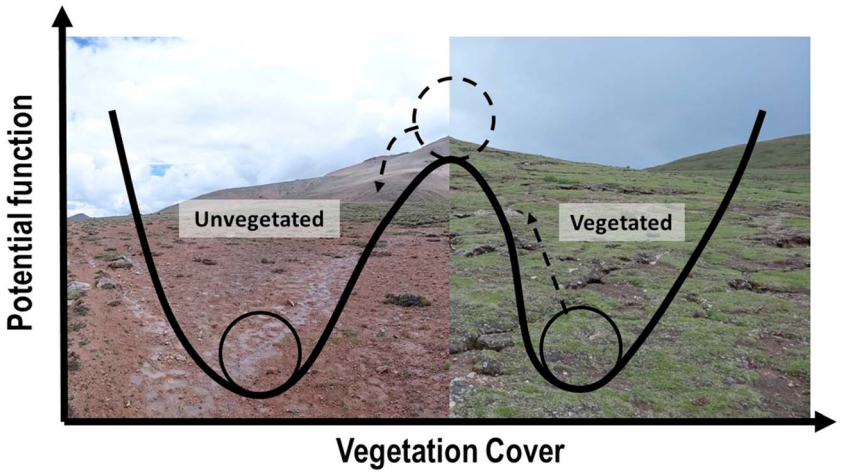

Figure 6. Proposed bistable ecosystem dynamics in *K. pygmea* meadows.

4. Discussion

Observational evidence indicates that the degradation of turfed soils leads to mineral soil exposure and erosion (Shao et al., 2011). Thus, we argue that these turf mats control the delivery of large amounts of sediment to the headwaters of major Asian rivers, including the Yangtze, Mekong, and Brahmaputra. Using cosmogenic ^{10}Be, Lal et al. (2004) have estimated rates of erosion ~0.01 mm/year (0.003–0.03 mm/year) from the interior of the Tibetan Plateau. For the eastern margin of the Plateau, which has more relief than the central portion, denudation rates of $>$0.1 mm/year have been estimated by others (e.g., Godard et al., 2010; Kirby et al., 2002; Liu-Zeng et al., 2011; Ouimet et al., 2010). For a 300-m slope (n = 200), our results indicate erosion over two centuries, once significant turf degradation has occurred, of order 0.1 mm/year (Figure 5). We do not mean to imply by this comparison that turf degradation controls all erosion on the plateau. Rather, we suggest that in areas where it normally would occur, its absence can result in erosion rates of the same order as observed elsewhere.

Our model shows that degradation of the turf through erosion occurs relatively rapidly upon creation of the hexagons. Once the process has been triggered through cracking, the landscape can undergo an unavoidable trajectory of degradation until the whole turf has been removed. It remains unclear whether (and to what extent) *K. pygmaea* turfs can reestablish on a thin, degraded soil. If establishment takes more than a few decades, the process may be irreversible within the timescale of a few human generations. Thus, the system is likely to exist in two possible stable configurations (Figure 6), unbroken turf and bare mineral soil, with the fragments of turf observed in many places today representing a transient state.

Kobresia pygmaea acts as an ecosystem engineer (Jones et al., 1996) in the sense that by contributing to soil stabilization, the mats create and maintain their own habitat. Thus, a positive feedback exists between *K. pygmaea* turfs and the underlying soil. Positive feedback in ecosystems are known for their ability to induce bistable dynamics (e.g., Walker & Salt, 2006), whereby the system is stable in two different configurations (i.e., both with turfs stabilizing the soil mantle and with degraded barren soils; Figure 6). If this were the case, *K. pygmaea* turfs would have a limited resilience and would be prone to a transition to a stable degraded state that would likely be irreversible or have long recovery times. Such a transition would be associated with the loss of important ecosystem services, including grazing for the principal livestock, yaks. Moreover, as the dominant ecosystem on the Earth's "Third Pole," these meadows are critical for mediating land-atmosphere interactions in this climatically pivotal region. The irreversible loss of the meadows, and their replacement with bare slopes, represents a significant alteration of energy, water, and mass fluxes at the surface. With expected intense climate change in the Tibetan Plateau (~12% increase in precipitation and ~4.1°C increase in temperature by the end of the century (Intergovernmental Panel on Climate Change, 2013), the study of the dynamics of these systems is essential to set benchmarks for future studies and to inform modeling at scales ranging from the hillslope to the globe.

Acknowledgments

All data and parameters for the model presented here are included in the text.

References

Brown, L. C., & Foster, G. R. (1987). Storm erosivity using idealized intensity distributions. *Transactions of ASAE*, *30*(2), 379–386. https://doi.org/10.13031/2013.31957

Chow, V. T. (1959). *Open channel hydraulics* (p. 680). New York: McGraw-Hill College.

Godard, V., Lavé, J., Carcaillet, J., Cattin, R., Bourlès, D., & Zhu, J. (2010). Spatial distribution of denudation in Eastern Tibet and regressive erosion of plateau margins. *Tectonophysics*, *491*(1–4), 253–274. https://doi.org/10.1016/j.tecto.2009.10.026

Hoffmans, G., Akkerman, G. J., Verheij, H., van Hoven, A., & van der Meer, J. (2009). The erodibility of grassed inner dike slopes against wave overtopping. In J. M. Smith (Ed.), *Coastal Engineering 2008; Proceedings of the 31st International Conference on Coastal Engineering* (pp. 3224–3236). Hamburg, Germany: World Scientific Publishing Company.

Holzner, W., & Kriechbaum, M. (1998). Man's impact on the vegetation and landscape in the Inner Himalaya and Tibet. In M. Elvin & T. J. Liu (Eds.), *Sediments of Time: Environment and Society in Chinese History* (pp. 53–106). Cambridge: Cambridge University Press.

Intergovernmental Panel on Climate Change (2013). *Climate change 2013: The physical science basis. Working Group I contribution to the IPCC 5th Assessment Report* (p. 1552). Cambridge: Cambridge University Press.

Jones, C., Lawton, J., & Shachak, M. (1996). Organisms as ecosystem engineers. In *Ecosystem Management* (pp. 130–147). Springer: New York.

Kirby, E., Reiners, P. W., Krol, M. A., Whipple, K. X., Hodges, K. V., Farley, K. A., et al. (2002). Late Cenozoic evolution of the eastern margin of the Tibetan Plateau: Inferences from 40Ar/39Ar and (U-Th)/He thermochronology. *Tectonics*, *21*(1), 1001. https://doi.org/10.1029/2000TC001246

Klein, J. A., Harte, J., & Zhao, X.-Q. (2007). Experimental Warming, not Grazing, Decreases Rangeland Quality on the Tibetan Plateau. *Ecological Applications*, *17*(2), 541–557. https://doi.org/10.1890/05-0685

Kottegoda, N. T., & Rosso, R. (1997). *Probability, statistics, and reliability for civil and environmental engineers*. New York: McGraw-Hill.

Koutsoyiannis, D., & Foufoula-Georgiou, E. (1993). A scaling model of a storm hyetograph. *Water Resources Research*, *29*, 2345–2361. https://doi.org/10.1029/93WR00395

Lachenbruch, A. H. (1961). Depth and spacing of tension cracks. *Journal of Geophysical Research*, *66*, 4273–4292. https://doi.org/10.1029/JZ066i012p04273

Lal, D., Harris, N. B. W., Sharma, K. K., Gu, Z., Ding, L., Liu, T., et al. (2004). Erosion history of the Tibetan Plateau since the last interglacial: constraints from the first studies of cosmogenic 10Be from Tibetan bedrock. *Earth and Planetary Science Letters*, *217*(1–2), 33–42. https://doi.org/10.1016/S0012-821X(03)00600-9

Liu-Zeng, J., Wen, L., Oskin, M., & Zeng, L. (2011). Focused modern denudation of the Longmen Shan margin, eastern Tibetan Plateau. *Geochemistry, Geophysics, Geosystems*, *12*, Q11007. https://doi.org/10.1029/2011GC003652

Miehe, G., Miehe, S., Böhner, J., Kaiser, K., Hensen, I., Madsen, D., et al. (2014). How old is the human footprint in the world's largest alpine ecosystem? A review of multiproxy records from the Tibetan Plateau from the ecologists' viewpoint. *Quaternary Science Reviews*, *86*, 190–209. https://doi.org/10.1016/j.quascirev.2013.12.004

Miehe, G., Miehe, S., Kaiser, K., Jianquan, L., & Zhao, X. (2008). Status and dynamics of the Kobresia pygmaea ecosystem on the Tibetan Plateau. *Ambio*, *37*(4), 272–279. https://doi.org/10.2307/25547897

Ouimet, W., Whipple, K., Royden, L., Reiners, P., Hodges, K., & Pringle, M. (2010). Regional incision of the eastern margin of the Tibetan Plateau. *Lithosphere*, *2*(1), 50–63. https://doi.org/10.1130/l57.1

Renard, K. G., Foster, G. R., Weesies, G. A., McCool, D., & Yoder, D. (1997). *Predicting soil erosion by water: A guide to conservation planning with the Revised Universal Soil Loss Equation (RUSLE)*, *Agriculture Handbook No. 703*. Washington: U. S. Department of Agriculture.

Renard, K. G., Foster, G. R., Weesies, G. A., & Porter, J. P. (1991). RUSLE: Revised universal soil loss equation. *Journal of Soil and Water Conservation*, *46*(1), 30–33.

Rodriguez-Iturbe, I., Cox, D. R., & Isham, V. (1987). Some models for rainfall based on stochastic point processes. *Proceedings of the Royal Society of London. A. Mathematical and Physical Sciences*, *410*(1839), 269–288. https://doi.org/10.1098/rspa.1987.0039

Shao, Q., Xiao, T., Liu, J., & Qi, Y. (2011). Soil erosion rates and characteristics of typical alpine meadow using 137Cs technique in Qinghai-Tibet Plateau. *Chinese Science Bulletin*, *56*(16), 1708–1713. https://doi.org/10.1007/s11434-011-4477-0

Walker, B., & Salt, D. (2006). *Resilience thinking: sustaining ecosystems and people in a changing world*. Washington, DC: Island Press.

Xiong, D., Shi, P., Sun, Y., Wu, J., & Zhang, X. (2014). Effects of grazing exclusion on plant productivity and soil carbon, nitrogen storage in alpine meadows in northern Tibet, China. *Chinese Geographical Science*, *24*(4), 488–498. https://doi.org/10.1007/s11769-014-0697-y

Zhou, T., Yu, R., Chen, H., Dai, A., & Pan, Y. (2008). Summer precipitation frequency, intensity, and diurnal cycle over China: A comparison of satellite data with rain gauge observations. *Journal of Climate*, *21*(16), 3997–4010. https://doi.org/10.1175/2008JCLI2028.1